Environmental Science & Technology

ARTICLE

pubs.acs.org/est

Oxidation State and Local Structure of Plutonium Reacted with Magnetite, Mackinawite, and Chukanovite

Regina Kirsch,[*,†,‡] David Fellhauer,[§] Marcus Altmaier,[∥] Volker Neck,[⊥,∥] Andre Rossberg,[†] Thomas Fanghänel,[§] Laurent Charlet,[‡] and Andreas C. Scheinost[*,†]

[†]Institut für Radiochemie, Helmholtz Zentrum Dresden Rossendorf, Postfach 510119, 01314 Dresden, Germany

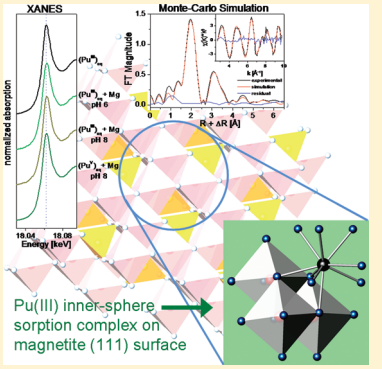
[‡]Institute des Sciences de la Terre, Université Joseph Fourier, CNRS, BP 53, 38041 Grenoble, France

[§]European Commission, Joint Research Center, Institute for Transuranium Elements, P.O. Box 2340, 76125 Karlsruhe, Germany

[∥]Institut für Nukleare Entsorgung, Karlsruhe Institute of Technology, Postfach 3640, 76021 Karlsruhe, Germany

Supporting Information

ABSTRACT: Due to their redox reactivity, surface sorption characteristics, and ubiquity as corrosion products or as minerals in natural sediments, iron(II)-bearing minerals control to a large extent the environmental fate of actinides. Pu-L_{III}-edge XANES and EXAFS spectra were used to investigate reaction products of aqueous ^{242}Pu(III) and ^{242}Pu(V) reacted with magnetite, mackinawite, and chukanovite under anoxic conditions. As Pu concentrations in the liquid phase were rapidly below detection limit, oxidation state and local structure of Pu were determined for Pu associated with the solid mineral phase. Pu(V) was reduced in the presence of all three minerals. A newly identified, highly specific Pu(III)-sorption complex formed with magnetite. Solid PuO_2 phases formed in the presence of mackinawite and chukanovite; in the case of chukanovite, up to one-third of plutonium was also present as Pu(III). This highlights the necessity to consider, under reducing anoxic conditions, Pu(III) species in addition to tetravalent PuO_2 for environmental risk assessment. Our results also demonstrate the necessity to support thermodynamic calculations with spectroscopic data.



INTRODUCTION

Plutonium is the major transuranium actinide in civil and military nuclear waste. It is of environmental concern because of its high radiotoxicity and the long half-life of relevant nuclides (^{239}Pu: 24 100 a, ^{242}Pu: 375 000 a, ^{244}Pu: 8.0×10^7 a).[1] The solubility and complexation behavior of plutonium in aqueous systems and therefore its environmental fate are highly oxidation state dependent.[2] Due to its predominance over a wide pe/pH range and the possibility of colloid formation,[3,4] PuO_2 is considered one of the most important solids for Pu risk assessment. Under reducing conditions in the acidic to neutral pH range and particularly in the presence of dissolved Fe(II) or Fe(II)-bearing minerals, however, Pu(III) is relevant and compared to Pu(IV) often forms more soluble species.[5−7] Generally, sorption on minerals and redox reaction with them are among the individual processes that largely impact migration behavior of plutonium.[8] Since iron minerals form as corrosion products of zerovalent iron and steel (the first engineered physical barrier to Pu mobilization in most nuclear waste repository concepts) and are present in many "far field" barriers (clay or granite), their reactions with plutonium are of particular importance. Depending on redox conditions, groundwater composition, and microbial activity, Fe(II), Fe(III), or mixed Fe(II)−Fe(III) minerals such as magnetite ($Fe^{II}Fe^{III}_2O_4$), maghemite (γ-Fe_2O_3), green rust, siderite ($FeCO_3$), chukanovite ($Fe_2(CO)_3(OH)_2$), and mackinawite (FeS) have been observed as corrosion products of steel.[9−11] Magnetite and mackinawite are widespread in natural sediments;[12,13] chukanovite was found to result from microbial reduction of magnetite and lepidocrocite.[14,15] Sorption of plutonium to iron[16−19] and manganese minerals[16,20] can be accompanied by redox processes, leading to reduction or oxidation of the initial Pu oxidation state. For example, sorption of Pu(V) to hematite, goethite, and magnetite was found to be accompanied by surface mediated reduction to Pu(IV).[16−19,21] While the reductive capacity of the Fe(II)−Fe(III) mixed valence spinel magnetite is well-known,[22,23] the reduction of Pu(V) with iron(III) minerals hematite and goethite was attributed to the presence of traces of Fe(II) or to a stabilization of solid-state Pu(IV).[18] Due to a lack of measured redox potentials and Fe(II) concentrations, it is not possible to clearly link these observations with thermodynamic predictions on Pu oxidation states. Also, in many of the Pu-mineral interaction studies, the oxidation state distribution of plutonium on the solid phase and in solution was assessed indirectly, that is after leaching of plutonium from the solid phase and applying solvent extraction schemes to separate the different Pu oxidation states.

Received: February 24, 2011
Accepted: July 14, 2011
Revised: July 8, 2011
Published: July 14, 2011

Downloaded via LOS ALAMOS NATL LABORATORY on October 24, 2024 at 21:13:14 (UTC).
See https://pubs.acs.org/sharingguidelines for options on how to legitimately share published articles.

 © 2011 American Chemical Society

Table 1. Experimental Conditions at the Start and End of the Reaction Period for Pu(III) and Pu(V) ($[Pu(tot)]_{initial}$ $1.3 \pm 0.1 \times 10^{-5}$ M) Reacted with Magnetite, Mackinawite, and Chukanovite

sample	pH_{sus} [a] $_{start}$ [c]	pH_{cen} [b] $_{start}$	$pe_{susstart}$	$pe_{censtart}$	pH_{susend} [c]	pH_{cenend}	pe_{susend}	pe_{cenend}	$[Fe(II)]_{start}$ [μmol/L]	$[Fe(II)]_{end}$ [μmol/L]	$[Fe(III)]_{start}$ [μmol/L]
Pu(III) + magnetite, pH 6	6.3	6.1	−1.2	−0.2	6.1	5.5	−1.3	2.9	4940	3130	199
Pu(III) + magnetite, pH 8	7.9	7.7	−5.0	−2.5	7.9	7.4	−4.9	2.1	22.7	21.8	bdl[e]
Pu(V) + magnetite, pH 8	7.7	7.9[d]	−4.8	1.5[d]	7.9	7.2	−5.0	2.4	15.1	19.3	bdl
Pu(V) + mackinawite, pH 8	8.2	8.4[d]	−5.2	−5.7[d]	8.0	8.4	−4.9	−2.1	16.6	8.0	bdl
Pu(V) + chukanovite, pH 8	8.4	8.7[d]	−4.9	−5.0[d]	8.4	8.0	−5.8	−3.3	13.9	69.2	1.5

[a] sus: pH or pe measured in suspension. [b] cen: pH or pe measured after centrifugation. [c] start, end: start values measured 1 day after addition of plutonium to the mineral suspensions, end values measured at maximum 1 day prior to harvesting. [d] Values acquired 1 day before addition of plutonium. [e] bdl: below detection limit, detection limit for Fe(II) and Fe(III) is approximately 1×10^{-7} mol/L $[Fe(III)]_{end}$ was below detection limit for all samples

To investigate redox reactions of Pu with chemically and structurally differing Fe(II)-bearing minerals under anoxic conditions, we chose magnetite (an iron oxide), mackinawite (an iron sulfide), and chukanovite (an iron hydroxy carbonate), which after its first identification in 1976[24] was largely overlooked until recently.[9,11] The magnetite and mackinawite studies were performed in carbonate free solutions. Cryogenic X-ray absorption spectroscopy (XAS) was used to assess *in situ* oxidation states and local structures of resulting Pu-solid phases or surface complexes. To permit linking of thermodynamic modeling to Pu oxidation state distribution derived from X-ray absorption near edge structure (XANES) and extended X-ray absorption fine structure (EXAFS) spectra, care was taken to characterize sample redox conditions (pe, pH, [Fe(II)]). While the reactions of U(VI)[25] and Np(V)[26] with mackinawite have been investigated previously, we are not aware of any similar experiment involving Pu. The reduction of Pu(V) with magnetite[17] has been investigated in detail as a function of pH but not with XAS and not under anoxic conditions, thereby limiting the applicability of the results to anoxic conditions typical of deep-underground repositories and groundwater aquifers. The reaction of Pu with chukanovite has, to our knowledge, never been investigated.

MATERIALS AND METHODS

Generally, all sample manipulations, including mineral synthesis and washing, UV−vis measurements, and preparation of samples for XAS measurements, were carried out under anoxic conditions in nitrogen or argon glove-boxes with 0−10 ppmv O_2. Experiments were carried out at RT (23 ± 3 °C); deionized (18.2 MΩ Milli-Q), degassed (O_2 and CO_2 free) water was used for all purposes.

Mineral Synthesis and Characterization. Magnetite (Fe_3O_4), mackinawite (FeS), and chukanovite ($Fe_2(CO_3)(OH)_2$) were synthesized as detailed in the Supporting Information (SI). The identity of the reaction products was confirmed using synchrotron powder XRD (magnetite, mackinawite,[27] chukanovite Figure S1). Specific surfaces areas (Table S2) were determined with the BET method[28] (for details see the SI).

Preparation of Pu-Stock Solutions. A well characterized 2.2×10^{-2} mol/L Pu(VI) stock solution was obtained after purification and electrochemical oxidation. The isotopic composition of plutonium was 99.4 wt.% Pu-242, 0.58 wt.% Pu-239, 0.005 wt.% Pu-238, and 0.005 wt.% Pu-241; interfering radiolytic reactions can therefore be excluded. Stock solutions of 8.6×10^{-4} M Pu(V) and 7.3×10^{-4} M Pu(III) were then prepared electrolytically in 0.5 M NaCl and 0.1 M $NaClO_4$, respectively. Prior to addition of Pu(V) or Pu(III) to mineral suspensions, the pH was raised by addition of 1 or 4 M NaOH to pH 3.0 for Pu(V) and to pH 2.0 for Pu(III), and the initial oxidation state was confirmed by UV−vis spectroscopy using a diode array spectrophotometer (Carl Zeiss Jena). The added Pu(V) stock solution contained up to 2% of Pu(VI), no other oxidation states or Pu(IV) colloids could be identified in the Pu(III) stock solution (wavelengths used for quantification were 601 nm for Pu(III), 569 nm for Pu(V), 830 nm for Pu(VI)). Total [Pu] in the stock solutions was determined using liquid scintillation counting (LSC). Similar [Pu] before and after 10 kD (∼2 nm) ultrafiltration (Microsep 10k Omega filters) indicated the absence of significant amounts of PuO_2 colloids in the stock solutions.

Sample Preparation and Wet Chemical Characterization. Relevant experimental values are summarized in Table 1. One week prior to Pu addition, the mineral suspensions were adjusted to an ionic background of 0.1 M NaCl. For magnetite and mackinawite, the suspension pH was adjusted, while the chukanovite suspension was used as is. Pu(V) or Pu(III) stock solutions were added to the mineral suspensions to obtain [Pu(tot)] of $1.3 \pm 0.1 \times 10^{-5}$ M; no significant changes in sample pH were observed. Samples were allowed to react in the dark for 41 (Pu(V)) and 39 days (Pu(III)). Wet pastes of the minerals were then separated from the suspension by centrifugation and transferred into double confinement PE XAS sample holders that were heat sealed and subsequently kept shock frozen in a liquid nitrogen dewar until measurement. [Fe(II)] and [Fe(total)] concentrations were determined using the Ferrozine method[29] and [Pu] with LSC after 10kD ultrafiltration of aliquots of the mineral suspensions. pH and pe were determined in two ways: in suspension and in the clear supernatant after centrifugation of an aliquot of the sample, with the solid at the bottom of the centrifuge tube. During pH measurements, a stable potential was usually reached within 5 min. Redox potentials were read after 10 to 15 min in suspensions and after 15 to 30 min in centrifuged samples (for a discussion of different pH and pe measurement approaches, see the SI, p S4). pH was measured using a combined glass electrode with the ROSS reference system calibrated against pH standard buffer solutions (Merck). Redox potentials E(V) were measured with a Pt-combination electrode with Ag/AgCl reference system (Metrohm, reference electrolyte 3 M KCl) and converted into Eh according to Eh = E(V) + 0.208 V at 23 °C and 3 M KCl. pe is subsequently calculated according to pe = (F/(2.303 RT)) · Eh.

XAS Spectra Acquisition and Data Treatment. XANES and EXAFS spectra were acquired in fluorescence mode at the Pu-L_{III}

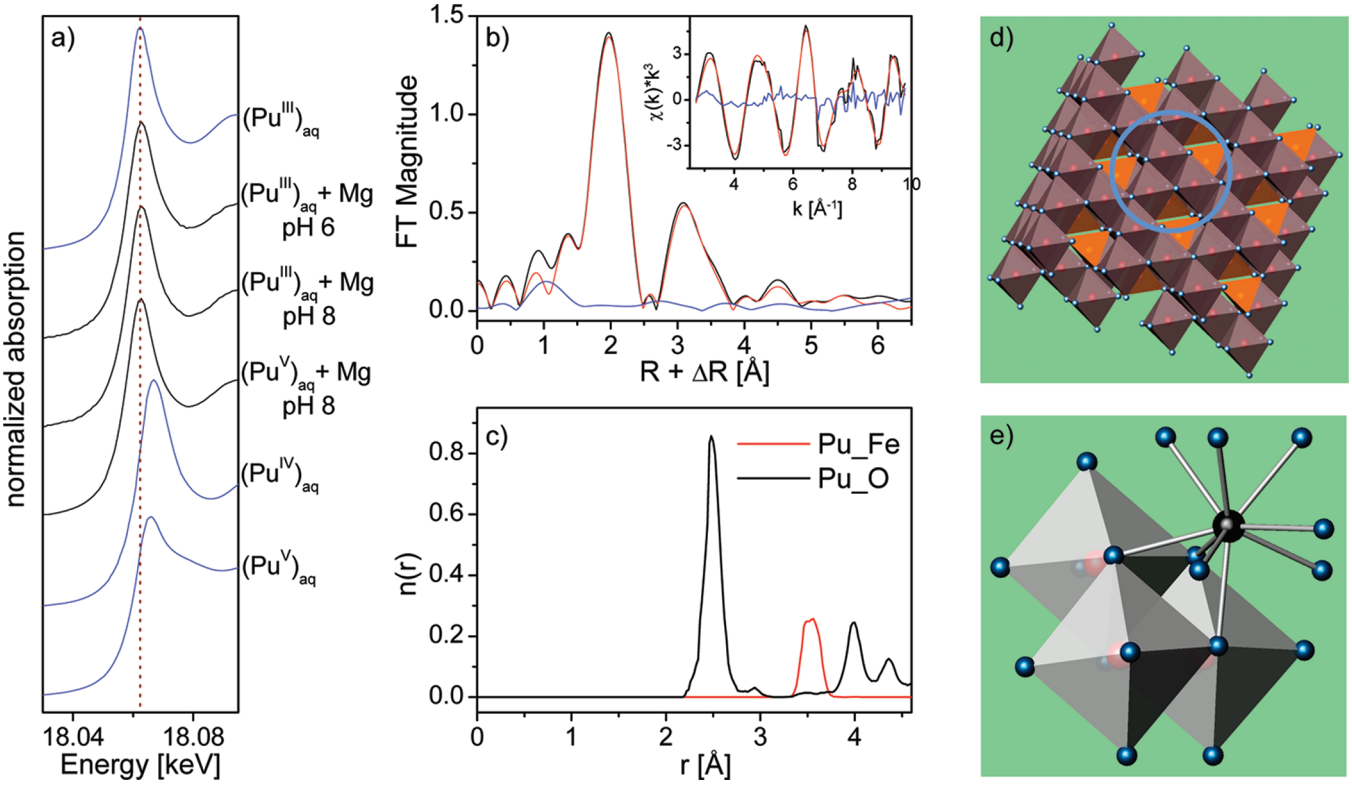


Figure 1. a) Experimental Pu-L_{III} XANES spectra of Pu reacted with magnetite (black) and $(Pu^{III})_{aq}$, $(Pu^{IV})_{aq}$, and $(Pu^{V})_{aq}$ for reference (blue). b) Experimental Pu-L_{III} EXAFS spectrum of $(Pu^{V})_{aq}$ + Mg, pH 8 sample (black) and theoretical spectrum (red) resulting from radial refinement by MC simulation, FT, and chi-spectrum (inset) (blue - residual). c) Pu−O and Pu−Fe radial pair distribution functions resulting from radial refinement. d) Octahedrally terminated (111) face of magnetite with one out of 7 possible positions for Pu(III) sorption marked by a blue circle. e) Sorption complex structure of Pu(III) on edge-sharing FeO_6-octahedra (Pu − black, O − blue, Fe − red).

edge (18.057 keV) at the Rossendorf Beamline at ESRF, France. During the measurement, samples were kept at 15 K using a closed-cycle He cryostat, thereby reducing thermal disorder and preventing beam-induced oxidation state changes. Details of experimental setup and treatment of spectra are given in the Supporting Information.

Reference spectra of acidic $(Pu^{III})_{aq}$, $(Pu^{IV})_{aq}$ and $(Pu^{V})_{aq}$ (measured at RT, courtesy of Ch. Den Auwer, CEA, Marcoule, France) and of crystalline PuO_2(cr) (measured at 15 K, courtesy of Ph. Martin, CEA, Cadarache, France)[30] had been measured in transmission mode and at the same beamline. Photon energies of the inflection points of absorption edges and white line maxima (peak positions) were determined for all sample and reference spectra (Table S3). The EXAFS data were fit with WinXAS[31] using theoretical backscattering amplitudes and phase shifts calculated with FEFF 8.2[32,33] on clusters (R_{max} = 8 Å) of PuO_2[34] and Pu_2O_3.[35] Uncertainties of the fits are about ±0.02 Å for distances and about ±20−25% for coordination numbers.[36] Statistical analysis of spectra (Eigen analysis and iterative target test) were performed with the ITFA program package.[37]

Thermodynamic Model. The diagram shown in Figure 3 was calculated using thermodynamic constants from the NEA TDB[38] where available. If data for Pu species were not available, complex formation constants and ion-interaction parameters (SIT coefficients) for ionic strength corrections were obtained from analogue actinide species. The thermodynamic model will be described in detail in a forthcoming article (Fellhauer et al., manuscript in preparation).

RESULTS AND DISCUSSION

For all five samples (Table 1), aqueous Pu concentrations dropped within 30 min and for the whole duration of the experiment to values near or below the detection limit of LSC ($\leq 1 \times 10^{-9}$ mol/L), thereby reaching uptake levels of ≥99.95%.

Reaction of Pu(III) and Pu(V) with Magnetite. Figure 1a shows Pu-L_{III}-edge XANES spectra of the Pu-magnetite samples along with $(Pu^{III})_{aq}$, $(Pu^{IV})_{aq}$, and $(Pu^{V})_{aq}$ references. The three Pu-magnetite samples are characterized by very similar edge and peak positions, irrespective of the initial Pu oxidation state and the reaction pH (Table S3) and strongly resemble the $(Pu^{III})_{aq}$ spectrum in position and shape (for description of XANES as a function of oxidation state, see the SI, 2.1). To quantify the oxidation state composition, the XANES region was analyzed using Iterative Target Testing (ITT).[37] ITT calculates the composition of sample spectra using factors that are extracted from all spectra analyzed together (sample and reference spectra). The reference spectra of $(Pu^{III})_{aq}$, $(Pu^{IV})_{aq}$, and $(Pu^{V})_{aq}$ were assumed to represent pure oxidation states and therefore assigned to 100% contents of the factors representing the respective states. For all three Pu-magnetite samples, Pu(III) contents higher than 90% are found (Table S4a). Pu(IV) and Pu(V) percent contents are not significant, given an absolute uncertainty of up to 10%. ITT was also applied to k^3-weighted $\chi(k)$-spectra obtained by back transform of the first peak in the Fourier Transform (FT). In this way, only the oxygen coordination shell is considered, and the differences in longer range structure between samples and references are excluded. The ITT results based on the

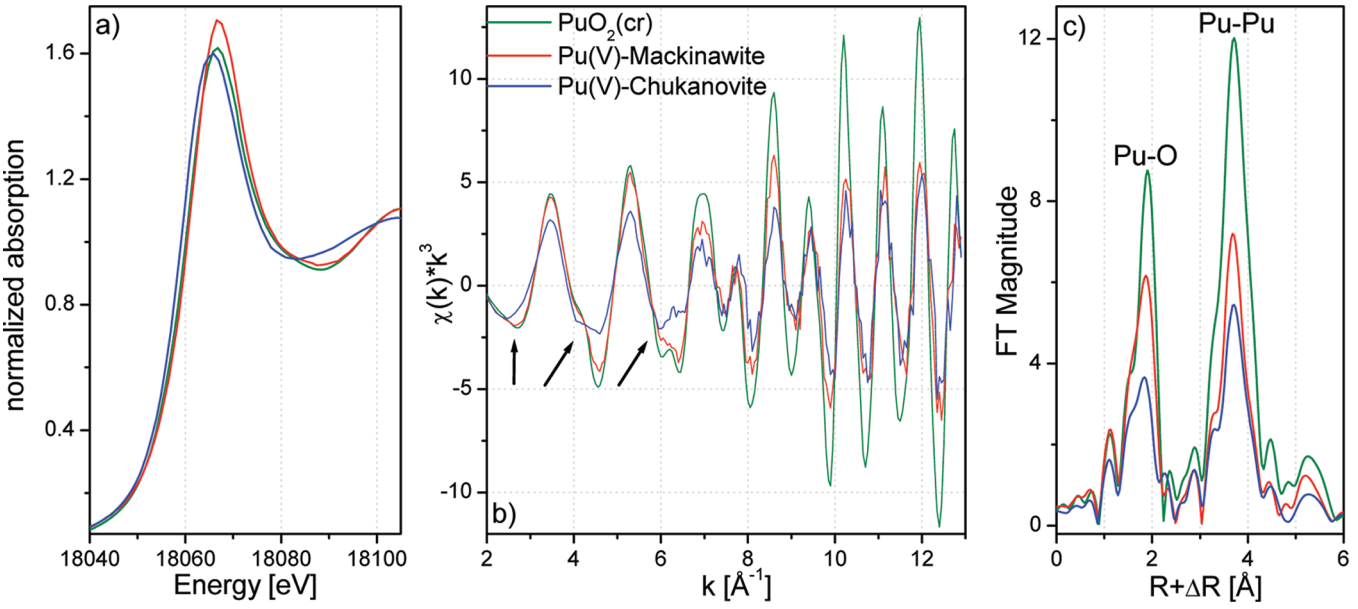


Figure 2. Experimetal Pu-L_{III} spectra of Pu(V)-Mack (red), Pu(V)-Chuk (blue), and PuO_2(cr) (green). a) XANES, b) $\chi(k) \times k^3$, c) Fourier transform ($3.0 < k < 12.6$ Å^{-1}).

such-obtained χ(k)-spectra confirm the prevalence of trivalent Pu (Table S4b). Shell fitting of the first FT peak yields Pu−O distances of 2.48 Å to 2.49 Å, characteristic of aqueous Pu(III) complexes[39−41] (Tables S5). In conclusion, edge and peak positions, ITT of the XANES and EXAFS regions and shell fitting of the first FT peak all suggest Pu(III) as the predominant oxidation state. Under the given experimental conditions (Table 1), the oxidation state of Pu after reaction with magnetite was independent of the initial oxidation state (III or V), suggesting that thermodynamic equilibrium has been attained. The fact that Powell et al.[17] found predominantly Pu(IV) is likely due to the presence of oxygen during their experiment. A similar impact of oxygen on the extent of reduction was observed by Nakata et al.[42] for the reaction between Np(V) and magnetite under aerobic and anaerobic conditions.

To elucidate the structure of the Pu(III) species on magnetite, shell fitting was extended to the FT peaks beyond the oxygen coordination sphere. A second shell could be fitted with backscattering from three to five Fe atoms at a distance of 3.54 Å, suggesting either a sorption complex or formation of a solid phase. To test the hypothesis of a sorption complex and to find a corresponding structure, FEFF-Monte Carlo (MC) modeling[43] was applied to the k^3-weighted EXAFS spectrum of the Pu(V) + magnetite, pH 8 sample (for modeling details, see the SI, 1.3). A box-procedure position-search was conducted using a model slab of magnetite ($18\times15\times5$ Å^3), exposing two (111) faces, one with octahedral and one with mixed tetrahedral/octahedral termination (Figure S2). One or two Pu atoms were allowed to move randomly and independently from each other in an empty $25\times25\times15$ Å^3 box surrounding the slab. For each Pu position in relation to the magnetite slab, a theoretical EXAFS spectrum was calculated with FEFF8.2 considering backscattering between Pu and magnetite; a constant scattering contribution for oxygen atoms of water molecules coordinated to aqueous Pu was then added. For 6, 7, or 8 coordinated water molecules only one geometrically specific position in relation to the magnetite slab, situated on the (111) surface with octahedral termination, was identified (Figure 1d). In the corresponding surface complex, one Pu atom is linked via three oxygen atoms to three edge-sharing FeO_6-octahedra. As Pu atoms remained always separated by more than 9 Å, a contribution of Pu−Pu backscattering to the experimental spectrum could be ruled out, thereby excluding formation of a dimeric surface complex or of Pu^{III}(hydr)oxide clusters. The position search was repeated using a different approach that minimizes the standard deviation (SD) of each new position compared to the previous one (see the SI) and lead to the identification of the same geometric position. The distances between the central Pu and the surrounding atoms in the thus identified structure of the sorption complex were refined by reverse Monte Carlo (RMC) simulation.[44,45] RMC allows small movements of all atoms surrounding Pu (up to 6.5 Å) to take structural disorder and possible relaxation effects of the magnetite surface into account (Figure 1e). During this radial refinement the number of coordinated water molecules was fixed at 6. As can be seen in Figure 1b, the resulting $\chi(k) \times k^3$ spectrum and the experimental spectrum are in excellent agreement. The refinement yields the Pu−O and Pu−Fe radial pair distribution functions (RPDF) (Figure 1c), wherein the first Pu−O peak corresponds to 9 oxygen atoms at 2.49 Å and the first Pu−Fe peak to three iron atoms at 3.54 Å. The Pu(III) position is close to an Fe-octahedral position and can be described as a tridentate, trinuclear, triple edge-sharing surface complex. Surface complexation at the octahedrally terminated (111) face geometry is in line with results from X-ray crystal truncation rod (CTR) diffraction from which 75% oxygen octahedral-iron (OOI) termination for magnetite (111) was deduced.[46] Due to the tridentate nature of the complex, it is likely to be very stable and play an important role in controlling Pu-magnetite reactions and Pu mobility.

Reaction of Pu(V) with Mackinawite and Chukanovite. XANES and EXAFS spectra of Pu(V) reacted with mackinawite (Pu(V)-Mack) and chukanovite (Pu(V)-Chuk) are similar to those of crystalline PuO_2(cr), suggesting the prevalence of tetravalent Pu in the samples and structural similarities with PuO_2(cr) (Figure 2). However, a higher white line (WL) intensity of the Pu(V)-Mack and a slight low-energy shift of

Table 2. Shell Fit of Pu(V)-Mack and PuO_2(cr) Samples with Fixed Coordination Numbers[c]

	Pu(V)-Mack			PuO_2(cr)		
path	CN	R [Å]	σ^2 [Å^2]	CN	R [Å]	σ^2 [Å^2]
Pu - O	8	2.32	0.0081[b]	8	2.33	0.0054[b]
Pu - Pu	12	3.81	0.0059	12	3.83	0.0032
Pu - O	24	4.40	0.0088	24	4.43	0.0061
Pu−O MS	8	4.64[a]	0.0081[b]	8	4.66[a]	0.0054[b]
Pu - Pu	6	5.36	0.0084	6	5.37	0.0068
Pu - Pu	24	6.69	0.0142	24	6.68	0.0087
	E_0-shift		5.83 eV	E_0-shift		6.81 eV
	residual		7.94%	residual		8.34%

[a] Fixed. [b] Correlated. [c] Fit carried out in R-space, for details see the SI, section 2.3.

the Pu(V)-Chuk spectrum compared to PuO_2(cr) are apparent (Figure 2a). While EXAFS frequencies and FT peak positions largely coincide for all three samples, the EXAFS amplitudes and FT peak heights decrease from PuO_2(cr) to Pu(V)-Chuk. Notable is the quasi congruence between the PuO_2(cr) and Pu(V)-Mack spectra below 7 Å^{-1} and between Pu(V)-Mack and Pu(V)-Chuk above 9 Å^{-1}. The EXAFS spectrum of Pu(V)-Chuk shows in the lower k-range significant additional differences to that of PuO_2(cr) (arrows in Figure 2b). As has been observed previously,[4,47] the WL peak heights of PuO_2 colloids are higher than the ones found for well crystallized PuO_2(cr). This fact precludes or at least significantly hampers the use of linear combination fitting or ITT to quantify PuO_2 in spectra containing a mixture of oxidation states. For the Pu(V)-Mack sample, the XANES region gives no indication for the presence of either tri- or pentavalent plutonium species (compare also Figure S3 and S4). When the Pu(V)-Mack and the PuO_2(cr) reference spectrum are fitted with a PuO_2 model in similar k-ranges (3.0−12.2 Å^{-1}) and with coordination numbers fixed to their crystallographic values, the goodness of fit obtained is similar for both spectra, suggesting that a PuO_2 solid phase formed in the Pu(V)-Mack sample (Table 2). The higher Debye−Waller factors (σ^2), corresponding to a higher mean square radial displacement of the backscattering atoms, indicate that the PuO_2 formed in the Pu(V)-Mack sample is characterized by higher structural disorder in the coordination and all further shells compared to calcinated PuO_2(cr). A fit of the first peak in the FT (at 1.8 Å in Figure 2c) with two oxygen shells was only possible when the σ^2 values for the hypothetical two distances were correlated and then yielded unrealistically small values (Table S11). However, we cannot exclude the presence of Pu−OH or Pu−OH_2 groups that might contribute to the higher structural disorder in the coordination shell of the PuO_2 contained in the Pu(V)-Mack sample.[4] No indication for the presence of Pu(V) could be derived from shell fitting.

By fitting the Pu(V)-Mack and PuO_2(cr) reference sample with adjustable coordination numbers, we also find similar Pu−Pu coordination numbers for both (Table S10). The number of backscattering Pu atoms at 3.82 Å decreases considerably with decreasing particle size only for PuO_2 particles with diameters below 2.5 nm. Between diameters of 8 and 3 nm, this coordination number decreases only from approximately 11.5 to 10.3 (calculated by assuming PuO_2 clusters, taking into account the change in Pu backscatterer numbers as a function of position in the cluster). As Pu−Pu coordination numbers for the PuO_2-(Mack) sample and the PuO_2(cr) reference are similar given the fit uncertainty of up to 25%, the only conclusion that can be drawn concerning particle size is that the PuO_2 particles formed with mackinawite likely have a diameter greater than the above-mentioned value of approximately 2.5 nm.

Despite the particularity of varying WL peak intensities for PuO_2 colloids, the edge and WL peak positions for such colloids are, in comparison to crystalline PuO_2(cr), shifted to higher energies.[47] The slight low-energy shift of the XANES region of the Pu(V)-Chuk sample therefore points to a contribution of a lower oxidation state to the spectrum. As is detailed in the SI (section 2.5), both the low energy shift in the absorption edge and the low k-range differences between Pu(V)-Chuk, Pu(V)-Mack, and PuO_2(cr) spectra (arrows in Figure 2) can be explained as resulting from the contribution of both Pu(III) and PuO_2 to the spectrum and the resulting interference between their corresponding backscattering waves (Figure S11). Tentative quantification with ITT using $(Pu^{III})_{aq}$ and PuO_2(cr) or the Pu(V)-Mack sample as references results for the XANES and EXAFS region in a Pu(III) content of 33% (Table S12) and also suggests that the Pu(V)-Mack spectrum might be a more suitable PuO_2 reference for the Pu(V)-Chuk spectrum than PuO_2(cr). Shell fitting applied to theoretical PuO_2-$(Pu^{III})_{aq}$-mixture spectra underscores the ITT-results concerning composition of the Pu-(V)-Chuk sample (SI, section 2.7) and highlights the limits of shell fitting to elucidate coordination shell structures in samples with mixed oxidation states.

Since a hypothetical solubility controlling Pu(III) phase, such as $Pu(OH)_3$, would lead to concentrations much higher than PuO_2(am,hyd) under our experimental conditions and furthermore would yield Pu concentrations higher than the LSC detection limit of 10^{-9} M, the observed low Pu concentration must be explained by a different Pu(III) species, most likely an inner-sphere sorption complex on the iron mineral phases. The present spectroscopic data, however, do not allow to differentiate between Pu(III) inner and outer sphere complexes or to identify the underlying mineral surface. The contribution of a heavy element backscatterer such as Fe or Pu to the spectrum of this hypothesized Pu(III)-sorption complex is however unlikely due to the overall spectral similarity of Pu(V)-Chuk to a theoretical $(Pu^{III})_{aq}$-PuO_2 mixture (Figure S11).

Impact of Mineral Phases on Reaction Products. For the three investigated reactions of Pu(V) with magnetite, mackinawite, and chukanovite at about pH 8, the concentration of dissolved Fe(II) and the pe values are on the same order of magnitude (Table 1) and thus, by themselves, can only partly account for the different reaction products, suggesting that the Pu redox state distribution found was influenced by the exact type of mineral surfaces present. For the (semi)conductors magnetite and mackinawite (magnetite: band gap of 0.1 eV,[48] mackinawite: metallic conductance[49]), a number of metal/metalloid contaminants are reduced by multielectron transfer reactions taking place at their surfaces (e.g., Se(IV) => Se(-II),[27] Cr(VI) => Cr-(III),[50,51] Sb(V) => Sb(III)[52]). With respect to Pu surface complexation, it is of relevance that, in contrast to magnetite, mackinawite surfaces are sulfur terminated,[49] which should considerably reduce their capability to serve as a ligand, as Pu is a hard Lewis acids and therefore oxyphilic.[53] If, for this reason, surface complexation with Pu(V) does not occur, electrons for a two-electron reduction from Pu(V) to Pu(III) cannot be provided directly by the mineral. The one electron necessary for the

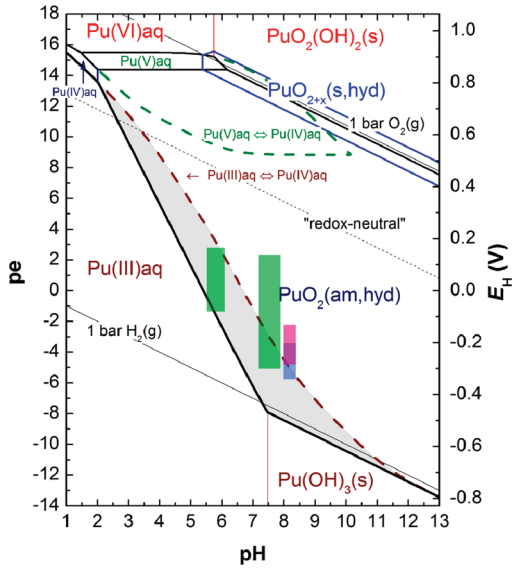


Figure 3. pe-pH predominance diagram for $[Pu] = 1 \times 10^{-5}$ M in 0.1 M NaCl. For construction of the full black lines, PuO_2(am,hyd) is the considered Pu(IV) equilibrium species. Dashed lines result from use of Pu(IV)aq instead of PuO_2(am,hyd) as redox partner for Pu(III)aq (brown) or Pu(V)aq (green). The gray shaded area highlights the increase of the Pu(III)aq predominance field when Pu(IV)aq instead of solid PuO_2(am,hyd) is the redox partner for Pu(III)aq. Final reaction conditions of the investigated mineral systems are depicted by superposed, colored bars (upper limit − supernatant values, lower limit − suspension values): magnetite (green), mackinawite (pink), and chukanovite (blue) systems (Table 1).

reduction from Pu(V) to Pu(IV) might be transferred from a Fe(II) aquo-ion or coadsorbed surface species. In the absence of a surface that allows formation of stable surface complexes, Pu(IV) precipitates as PuO_2. A similar behavior with mackinawite was observed for U(VI) that also does not form inner sphere surface complexes with surface sulfur atoms and, after partial reduction, forms a mixed U(VI)/U(IV) oxide solid phase.[25,54] In contrast, mackinawite removed only a small fraction of Np(V) from solution, which was reduced to Np(IV) present in sulfur coordinated inner-sphere surface complexes.[26] Should surface complexation between Pu and mackinawite have occurred in our experiment, it must be due to the absence of any identifiable Pu−S scattering path, very limited in extent.

As the mineral chukanovite was identified and characterized only recently,[55] not much is known about the mobility of electrons in its structure or reactivity toward other contaminants. We can only speculate that the partial reduction of Pu(V) to Pu(III) in chukanovite, but not in mackinawite suspensions, might be due to the complexation behavior of Pu, preferring oxygen over sulfur terminated surfaces, and thus be related to the thermodynamic stability of the respective surface complexes. Our data do not permit to draw a conclusion on whether electrons are provided from structural, coadsorbed or dissolved Fe(II).

Implications for Environmental Studies. Assessment of the long-term safety of nuclear waste repositories and contaminated sites are largely based on thermodynamic model calculations to predict the chemical behavior and potential release of radionuclides to the environment. Based upon macroscopic thermodynamic data for solids and aqueous species and assuming equilibrium conditions, solubility limits are calculated as a function of different geochemical boundary conditions (e.g., the Pu source term under near-field conditions). Using the same modeling approach and thermodynamic data, predominance fields for the expected Pu oxidation states and species can be predicted as a function of pe and pH conditions (Figure 3). As simplifications are made in the underlying chemical models (e.g., selection of species) and due to the lack of thermodynamic data for solids, surface complexes, and aqueous species, applying this approach to natural systems characterized by conditions overlapping with the predominance fields of different species is limited and associated with rather large uncertainties. Also, the precise characterization of reaction conditions of natural systems can be challenging and result in large uncertainties in measured pe and iron speciation (for a more detailed discussion, see SI, p S4).

For example, as indicated in Figure 3, the equilibrium line between Pu oxidation states three and four may be presented by the aquo-species $(Pu^{III})_{aq}$ on one side, and either the aquo-species $(Pu^{IV})_{aq}$ (brown dashed line) or colloidal PuO_2(am, hyd) (full black line) on the other side, resulting in a pH shift of more than one unit (gray shading in Figure 3). Bars shaded in green (magnetite), pink (mackinawite), and blue (chukanovite) delineate the pe values measured in clear supernatant (top) and in suspension (bottom), both values differing by up to seven pe units (Table 1). When comparing the spectroscopically observed oxidation states with the experimentally found pe/pH conditions (colored bars) and the predominance field of Pu oxidation states (Figure 3), it appears that the $(Pu^{III})_{aq}/(Pu^{IV})_{aq}$ redox equilibrium and the pe values determined in suspension come closest to our spectroscopic results. However, it cannot be excluded that the true equilibrium between the observed $(Pu^{III})_{adsorbed}$ species and Pu(IV) is shifted to higher pe values compared to the dashed brown $(Pu^{III})_{aq}/(Pu^{IV})_{aq}$ line, as relying on the pe values measured in the clear supernatant would suggest. The discrepancy between suspension and supernatant pe and pH values in comparison to Pu redox chemistry highlights the need to obtain reliable data for complex laboratory and natural conditions.

In order to derive better and more comprehensive quantitative models to predict Pu (redox) chemistry and Pu mobility in the environment, it will be necessary to include sorption effects into consistent thermodynamic models based upon data for aqueous species, Pu solids, iron and other common mineral solids, *and* Pu surface complexes on these minerals. To identify, characterize, and parametrize the processes taking place at mineral surfaces, a detailed understanding on a molecular level is needed and can be obtained by systematic application of advanced analytical/spectroscopic tools in combination to thermodynamic modeling. As we attempted to show, XAS allows in many cases to clearly identify Pu reaction products at the mineral surface, thereby enabling conclusions on the stability and expected environmental relevance of the identified species.

Our results highlight that Pu(III) is an important oxidation state in reducing anoxic environments; models based entirely on tetravalent Pu(IV) species are, therefore, inadequate. Consequently, to improve predictions on the fate of Pu in nuclear waste repositories and environmental systems, sorption of Pu(III) to relevant mineral surfaces should be investigated in more detail, also to lower the uncertainty of present predictions based upon analogy with other trivalent actinides, e.g. Am(III) and Cm(III). Relevant Pu(III) complexation and solubility constants should be determined to obtain more reliable quantitative models for Pu. Regarding the applicability of our results to natural settings, it should be considered that other factors (i.e., sorption of Pu on

additional mineral surfaces, interaction of Pu with dissolved ligands, variation of Pu/surface ratio or competitive sorption effects) can impact reaction outcomes and should be further investigated.

■ ASSOCIATED CONTENT

Supporting Information. Details are provided on mineral synthesis and characterization, XAFS spectra acquisition and data treatment, Monte Carlo simulation, sample reaction conditions, XANES analysis, ITT analysis and shell fitting, analysis of theoretical PuO_2−Pu(III) mixture spectra. This material is available free of charge via the Internet at http://pubs.acs.org.

■ AUTHOR INFORMATION

Corresponding Author

*E-mail: kirsch@esrf.fr (R.K.), scheinost@esrf.fr (A.C.S.).

Notes

[⊥]Deceased 01 August 2009.

■ ACKNOWLEDGMENT

This work has been financially supported by HZDR, KIT-INE, ISTerre (UJF/CNRS/INSU), PACHEM-Paris, and IUF. The research leading to these results has received funding from the European Community's Seventh Framework Programme (FP7/2007-2013) under Grant Agreement n° 232631. We are most grateful to Ch. Den Auwer (CEA, Marcoule) and Ph. Martin (CEA, Cadarache) for providing reference spectra, to T. Kisely (KIT-INE) for measuring BET specific surface areas, to D. Schild (KIT-INE) for Raman measurements, to A. Fernandez-Martinez (ILL) and G. Garbarino (ESRF) for XRD measurements, to D. Falkenberg (HZDR) for his flexibility in building XAFS double-confinement sample holders, to Ch. Hennig (HZDR) for helpful discussions, to X. Gaona and E. Wieland (PSI) who lent us a LN_2 transport dewar inset, and to the radioprotection responsibles at KIT-INE (Ch. Marquard) and ESRF (P. Colomp and Y. Pira) for the smooth collaboration before and during the XAFS experiment at ESRF.

■ REFERENCES

(1) Magill, J.; Pfennig, G.; Galy, J. *Chart of the nuclides*, 7th ed.; European Commission - DG Joint Research Centre - Institute of Transuranium Elements: Karlsruhe, 2006; p 44.

(2) Runde, W. The chemical interactions of actinides in the environment. *Los Alamos Sci.* **2000**, *26*, 392–411.

(3) Dardenne, K.; Seibert, A.; Denecke, M. A.; Marquardt, C. M. Plutonium(III,IV,VI) speciation in Gorleben groundwater using XAFS. *Radiochim. Acta* **2009**, *97* (2), 91–97.

(4) Rothe, J.; Walther, C.; Denecke, M. A.; Fanghanel, T. XAFS and LIBD investigation of the formation and structure of colloidal Pu(IV) hydrolysis products. *Inorg. Chem.* **2004**, *43* (15), 4708–4718.

(5) Rai, D.; Gorby, Y. A.; Fredrickson, J. K.; Moore, D. A.; Yui, M. Reductive dissolution of PuO_2(am): The effect of Fe(II) and hydroquinone. *J. Solution Chem.* **2002**, *31* (6), 433–453.

(6) Felmy, A. R.; Moore, D. A.; Rosso, K. M.; Qafoku, O.; Rai, D.; Buck, E. C.; Ilton, E. S. Heterogeneous reduction of PuO_2 with Fe(II): importance of the Fe(III) reaction product. *Environ. Sci. Technol.* **2011**, *45*, 3952–3958.

(7) Neck, V.; Altmaier, M.; Fanghanel, T. Solubility of plutonium hydroxides/hydrous oxides under reducing conditions and in the presence of oxygen. *C. R. Chimie* **2007**, *10* (10−11), 959–977.

(8) Kalmykov, S. N.; Kriventsov, V. V.; Teterin, Y. A.; Novikov, A. P. Plutonium and neptunium speciation bound to hydrous ferric oxide colloids. *C. R. Chim.* **2007**, *10* (10−11), 1060–1066.

(9) Saheb, M.; Descostes, M.; Neff, D.; Matthiesen, H.; Michelin, A.; Dillmann, P. Iron corrosion in an anoxic soil: Comparison between thermodynamic modelling and ferrous archaeological artefacts characterised along with the local in situ geochemical conditions. *Appl. Geochem.* **2010**, *25* (12), 1937–1948.

(10) El Hajj, H.; Abdelouas, A.; Grambow, B.; Martin, C.; Dion, M. Microbial corrosion of P235GH steel under geological conditions. *Phys. Chem. Earth* **2010**, *35*, 248–253.

(11) Lee, T. R.; Wilkin, R. T. Iron hydroxy carbonate formation in zerovalent iron permeable reactive barriers: Characterization and evaluation of phase stability. *J. Contam. Hydrol.* **2010**, *116* (1−4), 47–57.

(12) White, A. F.; Peterson, M. L.; Hochella, M. F. Electrochemistry and dissolution kinetics of magnetite and ilmenite. *Geochim. Cosmochim. Acta* **1994**, *58* (8), 1859–1875.

(13) Spadini, L.; Bott, M.; Wehrli, B.; Manceau, A. Analysis of the Major Fe Bearing Mineral Phases in Recent Lake Sediments by EXAFS Spectroscopy. *Aquat. Geochem.* **2003**, *9* (1), 1–17.

(14) Ona-Nguema, G.; Morin, G.; Wang, Y. H.; Menguy, N.; Juillot, F.; Olivi, L.; Aquilanti, G.; Abdelmoula, M.; Ruby, C.; Bargar, J. R.; Guyot, F.; Calas, G.; Brown, G. E. Arsenite sequestration at the surface of nano-$Fe(OH)_2$, ferrous-carbonate hydroxide, and green-rust after bioreduction of arsenic-sorbed lepidocrocite by Shewanella putrefaciens. *Geochim. Cosmochim. Acta* **2009**, *73* (5), 1359–1381.

(15) Kukkadapu, R. K.; Zachara, J. M.; Fredrickson, J. K.; Kennedy, D. W.; Dohnalkova, A. C.; McCready, D. E. Ferrous hydroxy carbonate is a stable transformation product of biogenic magnetite. *Am. Mineral.* **2005**, *90*, 510–515.

(16) Keeney-Kennicutt, W. L.; Morse, J. W. The redox chemistry of $Pu(V)O_2^+$ interaction with common mineral surfaces in dilute solutions and seawater. *Geochim. Cosmochim. Acta* **1985**, *49*, 2577–2588.

(17) Powell, B. A.; Fjeld, R. A.; Kaplan, D. I.; Coates, J. T.; Serkiz, S. M. $Pu(V)O_2^+$ adsorption and reduction by synthetic magnetite (Fe_3O_4). *Environ. Sci. Technol.* **2004**, *38* (22), 6016–6024.

(18) Powell, B. A.; Fjeld, R. A.; Kaplan, D. I.; Coates, J. T.; Serkiz, S. M. $Pu(V)O_2^+$ adsorption and reduction by synthetic hematite and goethite. *Environ. Sci. Technol.* **2005**, *39* (7), 2107–2114.

(19) Sanchez, A. L.; Murray, J. W.; Sibley, T. H. The adsorption of plutonium IV and V on goethite. *Geochim. Cosmochim. Acta* **1985**, *49*, 2297–2307.

(20) Powell, B. A.; Duff, M. C.; Kaplan, D. I.; Fjeld, R. A.; Newville, M.; Hunter, D. B.; Bertsch, P. M.; Coates, J. T.; Eng, P.; Rivers, M. L.; Sutton, S. R.; Triay, I. R.; Vaniman, D. T. Plutonium oxidation and subsequent reduction by Mn(IV) minerals in Yucca Mountain tuff. *Environ. Sci. Technol.* **2006**, *40* (11), 3508–3514.

(21) Kersting, A. B.; Zhao, P.; Zavarin, M.; Sylwester, E. R.; Allen, P. G.; Williams, R. W. Sorption of Pu(V) on Mineral Colloids. In *Colloidal-Facilitated Transport of Low-Solubility Radionuclides: A Field, Experimental, and Modeling Investigation*; Report UCRL-ID-149688; Kersting, A. B., Remus, P. W., Eds.; Lawrence Livermore National Laboratory: Livermore, CA, 2003.

(22) Duro, L.; El Aamrani, S.; Rovira, M.; De Pablo, J.; Bruno, J. Study of the interaction between U(VI) and the anoxic corrosion products of carbon steel. *Appl. Geochem.* **2008**, *23*, 1094–1100.

(23) White, A. F.; Peterson, M. L. Reduction of aqueous transition metal species on the surfaces of Fe(II)-containing oxides. *Geochim. Cosmochim. Acta* **1996**, *60* (20), 3799–3814.

(24) Erdös, E.; Altorfer, H. Ein dem Malachit aehnliches basisches Eisenkarbonat als Korrosionsprodukt von Stahl. *Werkst. Korros.* **1976**, *27*, 304–312.

(25) Moyes, L. N.; Parkman, R. H.; Charnock, J. M.; Vaughan, D. J.; Livens, F. R.; Hughes, C. R.; Braithwaite, A. Uranium uptake from aqueous solution by interaction with goethite, lepidocrocite, muscovite, and mackinawite: An X-ray absorption spectroscopy study. *Environ. Sci. Technol.* **2000**, *34* (6), 1062–1068.

(26) Moyes, L. N.; Jones, M. J.; Reed, W. A.; Livens, F. R.; Charnock, J. M.; Mosselmans, J. F. W.; Hennig, C.; Vaughan, D. J.; Pattrick, R. A. D. An X-ray absorption spectroscopy study of neptunium(V) reactions with mackinawite (FeS). *Environ. Sci. Technol.* **2002**, *36* (2), 179–183.

(27) Scheinost, A. C.; Kirsch, R.; Banerjee, D.; Fernandez-Martinez, A.; Zaenker, H.; Funke, H.; Charlet, L. X-ray absorption and photoelectron spectroscopy investigation of selenite reduction by FeII-bearing minerals. *J. Contam. Hydrol.* **2008**, *102*, 228–245.

(28) Brunauer, S.; Emmett, P. H.; Teller, E. Adsorption of gases in multimolecular layers. *J. Am. Chem. Soc.* **1938**, *60* (2), 309–319.

(29) Viollier, E.; Inglett, P. W.; Hunter, K.; Roychoudhury, A. N.; Van Cappellen, P. The ferrozine method revisited: Fe(II)/Fe(III) determination in natural waters. *Appl. Geochem.* **2000**, *15* (6), 785–790.

(30) Martin, P.; Grandjean, S.; Valot, C.; Carlot, G.; Ripert, M.; Blanc, P.; Hennig, C. XAS study of $(U_{1-y}Pu_y)O_2$ solid solutions. *J. Alloys Compd.* **2007**, *444*, 410–414.

(31) Ressler, T. WinXAS: a program for X-ray absorption spectroscopy data analysis under MS-Windows. *J. Synchrotron Radiat.* **1998**, *5*, 118–122.

(32) Ankudinov, A. L.; Ravel, B.; Rehr, J. J.; Conradson, S. D. Real Space Multiple Scattering Calculation of XANES. *Phys. Rev. B* **1998**, *58*, 7565.

(33) Ankudinov, A. L.; Bouldin, C.; Rehr, J. J.; Sims, J.; Hung, H. Parallel calculation of electron multiple scattering using Lanczos algorithms. *Phys. Rev. B* **2002**, *65* (10), 104107.

(34) Belin, R. C.; Valenza, P. J.; Reynaud, M. A.; Raison, P. E. New hermetic sample holder for radioactive materials fitting to Siemens D5000 and Bruker D8 X-ray diffractometers: application to the Rietveld analysis of plutonium dioxide. *J. Appl. Crystallogr.* **2004**, *37*, 1034–1037.

(35) Wulff, M.; Lander, G. H. Magnetic structure of Pu ground state in beta-Pu_2O_3. *J. Chem. Phys.* **1988**, *89* (5), 3295–3299.

(36) Denecke, M. A. Actinide speciation using X-ray absorption fine structure spectroscopy. *Coord. Chem. Rev.* **2006**, *250* (7−8), 730–754.

(37) Rossberg, A.; Reich, T.; Bernhard, G. Complexation of uranium(VI) with protocatechuic acid - application of iterative transformation factor analysis to EXAFS spectroscopy. *Anal. Bioanal. Chem.* **2003**, *376* (5), 631–638.

(38) Guillaumont, R.; Fanghänel, T.; Fuger, J.; Grenthe, I.; Neck, V.; Palmer, D. A.; Rand, M. H. *Update on the Chemical Thermodynamics of Uranium, Neptunium, Plutonium, Americium and Technetium*; Elsevier: Amsterdam, 2003.

(39) Allen, P. G.; Bucher, J. J.; Shuh, D. K.; Edelstein, N. M.; Reich, T. Investigation of aquo and chloro complexes of UO_2^{2+}, NpO_2^{+}, Np^{4+}, and Pu^{3+} by X-ray absorption fine structure spectroscopy. *Inorg. Chem.* **1997**, *36*, 4676–4683.

(40) Conradson, S. D.; Clark, D. L.; Neu, M. P.; Runde, W. H.; Tait, C. D. Characterizing the plutonium aquo ions by XAFS spectroscopy. *Los Alamos Sci.* **2000**, *26*, 418–421.

(41) Matonic, J. H.; Scott, B. L.; Neu, M. P. High-yield synthesis and single-crystal X-ray structure of a plutonium(III) aquo complex:$[Pu(H_2O)_9][CF_3SO_3]_3$. *Inorg. Chem.* **2001**, *40*, 2638–2639.

(42) Nakata, K.; Nagasaki, S.; Tanaka, S.; Sakamoto, Y.; Tanaka, T.; Ogawa, H. Sorption and reduction of neptunium(V) on the surface of iron oxides. *Radiochim. Acta* **2002**, *90* (9−11), 665–669.

(43) Rossberg, A.; Scheinost, A. C. Three-dimensional modeling of EXAFS spectral mixtures by combining Monte Carlo simulations and target transformation factor analysis. *Anal. Bioanal. Chem.* **2005**, *383* (1), 56–66.

(44) Gurman, S. J.; McGreevy, R. L. Reverse Monte-Carlo simulation for the analysis of EXAFS data. *J. Phys.: Condens. Matter* **1990**, *2* (48), 9463–9473.

(45) Winterer, M. Reverse Monte Carlo analysis of extended x-ray absorption fine structure spectra of monoclinic and amorphous zirconia. *J. Appl. Phys.* **2000**, *88* (10), 5635–5644.

(46) Petitto, S. C.; Tanwar, K. S.; Ghose, S. K.; Eng, P. J.; Trainer, T. P. Surface structure of magnetite (111) under hydrated conditions by crystal truncation rod diffraction. *Surf. Sci.* **2010**, *604*, 1082–1093.

(47) Conradson, S. D.; Abney, K. D.; Begg, B. D.; Brady, E. D.; Clark, D. L.; den Auwer, C.; Ding, M.; Dorhout, P. K.; Espinosa-Faller, F. J.; Gordon, P. L.; Haire, R. G.; Hess, N. J.; Hess, R. F.; Keogh, D. W.; Lander, G. H.; Lupinetti, A. J.; Morales, L. A.; Neu, M. P.; Palmer, P. D.; Paviet-Hartmann, P.; Reilly, S. D.; Runde, W. H.; Tait, C. D.; Veirs, D. K.; Wastin, F. Higher order speciation effects on plutonium L_3 X-ray absorption near edge spectra. *Inorg. Chem.* **2004**, *43* (1), 116–131.

(48) Cornell, R. M.; Schwertmann, U. *The Iron Oxides - Structure, Properties, Reactions, Occurrences and Uses Second, completely Revised and Extended ed.*; Wiley-VCH: Weinheim, 2003.

(49) Devey, A. J.; Grau-Crespo, R.; de Leeuw, N. H. Combined density functional theory and interatomic potential study of the bulk and surface structures and properties of the iron sulfide mackinawite (FeS). *J. Phys. Chem. C* **2008**, *112* (29), 10960–10967.

(50) Mullet, M.; Boursiquot, S.; Ehrhardt, J. J. Removal of hexavalent chromium from solutions by mackinawite, tetragonal FeS. *Colloids Surf., A* **2004**, *244* (1−3), 77–85.

(51) Jung, Y.; Choi, J.; Lee, W. Spectroscopic investigation of magnetite surface for the reduction of hexavalent chromium. *Chemosphere* **2007**, *68* (10), 1968–1975.

(52) Kirsch, R.; Scheinost, A. C.; Rossberg, A.; Banerjee, D.; Charlet, L. Reduction of antimony by nano-particulate magnetite and mackinawite. *Mineral. Mag.* **2008**, *71* (1), 185–189.

(53) *The chemistry of the actinide and transactinide elements*, 3rd ed.; Morss, L. R., Edelstein, N. M., Fuger, J., Eds.; Springer: Dordrecht, 2006; Vol. 4, pp 2524−2621.

(54) Hua, B.; Deng, B. Reductive immobilization of uranium(VI) by amorphous iron sulfide. *Environ. Sci. Technol.* **2008**, *42*, 8703–8708.

(55) Pekov, I. V.; Perchiazzi, N.; Merlino, S.; Vyacheslav, N.; Merlini, M.; Zadov, A. E. Chukanovite, $Fe_2(CO_3)(OH)_2$, a new mineral from the weathered iron meteorite Dronino. *Eur. J. Mineral.* **2007**, *19* (6), 891–898.